



Effects of urban land expansion on the regional meteorology and air quality of eastern China

W. Tao¹, J. Liu¹, G. A. Ban-Weiss², D. A. Hauglustaine³, L. Zhang⁴, Q. Zhang⁵, Y. Cheng⁶, Y. Yu⁷, and S. Tao¹

¹Laboratory for Earth Surface Processes, College of Urban and Environmental Sciences, Peking University, Beijing 100871, China

²Sonny Astani Department of Civil and Environmental Engineering, University of Southern California, CA, USA

³Laboratoire des Sciences du Climat et de l'Environnement, UMR8212, CEA-CNRS-UVSQ, Gif-sur-Yvette, France

⁴Laboratory for Climate and Ocean-Atmosphere Sciences, Department of Atmospheric and Oceanic Sciences, School of Physics, Peking University, Beijing 100871, China

⁵Center for Earth System Science, Tsinghua University, Beijing 100084, China

⁶Chinese Academy of Meteorological Sciences, Beijing, China

⁷Nanjing Municipal Environmental Monitoring Centre, Nanjing, Jiangsu 210013, China

Correspondence to: J. Liu (jfliu@pku.edu.cn)

Received: 27 January 2015 – Published in Atmos. Chem. Phys. Discuss.: 8 April 2015

Revised: 6 July 2015 – Accepted: 10 July 2015 – Published: 3 August 2015

Abstract. Rapid urbanization throughout eastern China is imposing an irreversible effect on local climate and air quality. In this paper, we examine the response of a range of meteorological and air quality indicators to urbanization. Our study uses the Weather Research and Forecasting model coupled with chemistry (WRF/Chem) to simulate the climate and air quality impacts of four hypothetical urbanization scenarios with fixed surface pollutant emissions during the month of July from 2008 to 2012. An improved integrated process rate (IPR) analysis scheme is implemented in WRF/Chem to investigate the mechanisms behind the forcing–response relationship at the process level. For all years, as urban land area expands, concentrations of CO, elemental carbon (EC), and particulate matter with aerodynamic diameter less than 2.5 microns (PM_{2.5}) tend to decrease near the surface (below ~ 500 m), but increase at higher altitudes (1–3 km), resulting in a reduced vertical concentration gradient. On the other hand, the O₃ burden, averaged over all newly urbanized grid cells, consistently increases from the surface to a height of about 4 km. Sensitivity tests show that the responses of pollutant concentrations to the spatial extent of urbanization are nearly linear near the surface, but nonlinear at higher altitudes. Over eastern China, each 10 % increase in nearby urban land coverage on average leads to a decrease of approximately 2 % in surface concentrations

for CO, EC, and PM_{2.5}, while for O₃ an increase of about 1 % is simulated. At 800 hPa, pollutants' concentrations tend to increase even more rapidly with an increase in nearby urban land coverage. This indicates that as large tracts of new urban land emerge, the influence of urban expansion on meteorology and air pollution would be significantly amplified. IPR analysis reveals the contribution of individual atmospheric processes to pollutants' concentration changes. It indicates that, for primary pollutants, the enhanced sink (source) caused by turbulent mixing and vertical advection in the lower (upper) atmosphere could be a key factor in changes to simulated vertical profiles. The evolution of secondary pollutants is further influenced by the upward relocation of precursors that impact gas-phase chemistry for O₃ and aerosol processes for PM_{2.5}. Our study indicates that dense urbanization has a moderate dilution effect on surface primary airborne contaminants, but may intensify severe haze and ozone pollution if local emissions are not well controlled.

1 Introduction

Urbanization refers to the growth of urban populations and the vast expansion of urban areas. According to the 2011 revision of the United Nations (UN) World Urbanization

Prospects, the global proportion of the population living in urban areas is likely to increase to 68 % (about 6.2 billion) by 2050, and the urban population in less developed regions will almost double from 2.7 billion in 2011 to 5.1 billion in 2050 (Heilig, 2012). The environmental side-effects of urbanization, such as inadvertent climate modification (Changnon, 1992) and air quality degradation (Mage et al., 1996), remain an important research topic with societal relevance.

The radiative, thermal, hydrologic, and aerodynamic properties of urban land surfaces are distinct from those of natural surfaces (e.g., forests, grassland), resulting in unique exchange processes of energy, moisture, and momentum with the ambient atmosphere and thus distinct climatic conditions in urban areas (Oke, 1987). The features of urban climate (e.g., urban heat island (UHI), wind profiles in the urban canopy layer) have been extensively observed, modeled and comprehensively reviewed (e.g., Arnfield, 2003; Kanda, 2007; Souch and Grimmond, 2006). The urban climate is characterized by multiple scales (Britter and Hanna, 2003; Fisher et al., 2006; Oke, 2006) e.g., flows in the roughness sublayer at micro-scale are not subject to Monin–Obukhov similarity relationships, whereas upper flows in the inertial layer are in equilibrium with the underlying surface, and can be described by mesoscale dynamics. Another feature of urban climatology is, heterogeneity, namely the high non-uniformities of roughness elements (e.g., impervious road, green belt) in urban areas make it rather complicated to generalize the urban flow details from one landscape to another (Fernando et al., 2001). Factors such as anthropogenic heat (Fan and Sailor, 2005), chemistry–climate feedbacks (Rosenfeld, 2000), and topography could alter the characteristics of urban climatic conditions, and the intensity of background wind speed or land-sea breezes could impact the structure of the urban boundary layer (Fisher et al., 2006; Rotach et al., 2002) and the ventilation conditions as well (Ryu et al., 2013; Yoshikado and Tsuchida, 1996).

Up to now, a number of urban canopy schemes have been developed (e.g., Coceal and Belcher, 2004; Di Sabatino et al., 2008; Harman et al., 2004; Luhar et al., 2014; Solazzo et al., 2010; Trusilova et al., 2013; Wang et al., 2011). Among them, four schemes with different complexities have been implemented in the mesoscale meteorological model (e.g., WRF) to account for the effects of urban areas on urban climate, namely bulk (BULK; Liu et al., 2006), a single-layer urban canopy model (SLUCM; Kusaka and Kimura, 2004), building effect parameterization (BEP; Martilli et al., 2002), and a building energy model (coupled to BEP, denoted as BEP + BEM; Salamanca et al., 2010). The BULK scheme parameterizes the urban surface with greater heat capacity, thermal conductivity, roughness length, and lower albedo than of natural land surfaces, and has been successfully employed in real-time weather forecasts (Liu et al., 2006). It could capture the features of urban synoptic conditions (Liao et al., 2014), and is being widely used for real-time mesoscale weather forecasting over urban areas (Sala-

manca et al., 2011). The last three schemes represent the urban geometry as street canyons with urban surfaces (i.e., walls, roofs, and roads), and the coupled WRF–SLUCM model reportedly has the ability to capture the UHI features in some megacities (Cui and de Foy, 2012; Lin et al., 2011; Miao et al., 2009). However, application of these urban canopy schemes requires specifying a vast number of urban canopy parameters and initial conditions (Chen et al., 2011), which are usually difficult to accurately configure and may change rapidly in developing countries.

Based on these urban canopy schemes, a series of modeling studies have investigated the effects of urban land-use changes on regional climate and air quality. Some key climatic effects of urbanization, e.g., an increase in mean surface temperature and PBL (planetary boundary layer) height, and decrease in humidity and wind speed, have been captured (e.g., Wang et al., 2012; Wang et al., 2013; Yang et al., 2012; Zhang et al., 2010), which in turn influence the concentrations of pollutants even if the anthropogenic emissions are held constant (Civerolo et al., 2007; De Meij et al., 2015; Wang et al., 2009; Yu et al., 2012). For instance, Kallos et al. (1993) indicated that land surface conditions play an important role in the development of local circulation and planetary boundary layer depth, and could govern the dispersal, transformation, and eventual removal of airborne pollutants. In addition, Ryu et al. (2013) found that the prevailing urban breeze in the afternoon brought O₃-rich and biogenic VOC-rich air masses from surrounding mountainous areas to the high-NO_x urban regions, resulting in a very high ozone episode in the Seoul metropolitan area.

To date, the characteristics and intrinsic mechanisms of the forcing exerted by urban land expansion on the atmospheric environment, including the burden of both primary and secondary pollutants, are still not well understood, particularly throughout eastern China. Recently, the Chinese government has relaxed its one-child policy to promote the long-term balanced development of the population, and has also launched an ambitious urbanization campaign. Therefore, it is expected that China will undergo continuous urban population growth and rapid urban land expansion in the coming decades. Land-use changes caused by new urban infrastructure are usually irreversible. If urban land expansion should exert adverse forcing on the ambient environment, mitigation strategies for climate and air quality improvement would be less easily implemented and more costly.

Using WRF/Chem, a mesoscale fully coupled air quality and meteorological model, this study addresses two key questions. (1) How sensitive are the meteorological conditions and the spatial distribution of airborne contaminants to urban land expansion? (2) What are the intrinsic mechanisms and dominant processes that drive urbanization-induced changes in atmospheric chemistry? We describe the methodology and the model in Sect. 2, and evaluate the model results in Sect. 3. In Sect. 4, we present the impact of urban land expansion on the distribution of key atmospheric

species. In Sect. 5, we investigate the individual processes contributing to these changes in atmospheric composition. Conclusions are provided in Sect. 6.

2 Methodology

2.1 Model description and configuration

We use WRF/Chem v3.5 (Grell et al., 2005) to simulate meteorological fields and atmospheric chemistry in four hypothetical urban land surface expansion scenarios in July for the 5 years from 2008 to 2012. We focus on summertime air quality because of the high ozone and other secondary pollutant levels. The modeling framework is constructed on a single domain of 100×100 cells with a 10 km horizontal grid spacing, and covers nine provinces in eastern and central China (Fig. 1). In this study, the physical options include the Lin microphysics scheme (Lin et al., 1983), RRTM long-wave radiation scheme (Mlawer et al., 1997), Goddard short-wave scheme (Kim and Wang, 2011), MM5 M–O surface layer scheme (Chen and Dudhia, 2001), YSU boundary layer scheme (Hong et al., 2006), New Grell cumulus scheme, and Unified Noah land surface model (Chen and Dudhia, 2001). The chemical options include the RADM2 chemical mechanism, MADE/SORGAM aerosol scheme, Madronich F-TUV photolysis scheme, and Megan biogenic emission scheme (Guenther et al., 2006). The $1.0^\circ \times 1.0^\circ$ NCEP Final Operational Global Analysis data (<http://rda.ucar.edu/datasets/ds083.2/>) have been processed to provide the meteorological initial conditions and boundary conditions. We utilize the modified 2008 IGBP (International Geosphere Biosphere Programme) MODIS 20-category 30 s land-use data, which is available from the WRF website (<http://www2.mmm.ucar.edu/wrf/users/>), to represent current land-cover conditions. Anthropogenic emission data are from the Multi-resolution Emission Inventory for China (MEIC), developed by Tsinghua University for the year 2010, which consists of the emission rates for each month from five sectors (agriculture, industry, power plants, residential, and transportation). The MEIC is a unit/technology-based, bottom-up emission model that covers ~ 700 anthropogenic emission source categories in China. It is an update of the emission inventory developed by the same group (Lei et al., 2011; Zhang et al., 2009). We used the MEIC 2010 data of the corresponding months as input for all simulations of 2008 through 2012, ignoring the year-to-year variation in emissions.

Predicted hourly ground level concentrations of CO, O₃, and particulate matter with aerodynamic diameter less than 2.5 microns (PM_{2.5}) are examined against observations made at five environmental monitoring sites, namely Nanjing Zhonghuamen site (NJ_ZHM, 118.78° E, 32.01° N), Nanjing Xianlin site (NJ_XL, 118.91° E, 32.11° N), Hangzhou Jiande site (HZ_JD, 119.28° E, 29.46° N), Hangzhou Yuhang site (HZ_YH, 119.99° E, 30.26° N) and Shanghai Pudong site

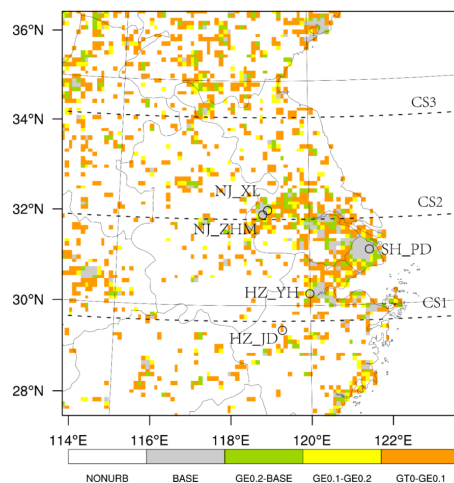


Figure 1. Schematic map of four idealized urban land expansion scenarios (i.e., BASE, GE0.2, GE0.1, and GT0). White denotes non-urban cells, and gray denotes urban cells in the BASE run. Other colors represent additional newly urbanized cells in GE0.2 (green), GE0.1 (yellow), and GT0 (orange) compared to previous urban land expansion scenarios. For example, urban cells in GE0.1 are gray, green, and yellow. Black open circles denote the five air quality monitoring sites. Black dashed lines running west–east demarcate the three vertical-zonal cross sections CS1, CS2, and CS3.

(SH_PD, 121.55° E, 31.22° N), as shown in Fig. 1. NJ_ZHM and NJ_XL are located in a mixed residential–educational area of Nanjing City, and the observation data (July 2012) are provided by Nanjing Municipal Environmental Monitoring Center. As NJ_ZHM and NJ_XL are located very close to each other, and cannot be distinguished at the current model resolution, we average the observation data of these two sites and report this as NJ. Both HZ_JD and HZ_YH are located at high schools in Hangzhou City, and the relevant observation data (April 2008) are from Jiang et al. (2012). SH_PD is located in the urban center of Pudong district, Shanghai, and relevant observation data (September 2012) are from Tie et al. (2013). Extra simulations for April 2008 and September 2012 have been conducted for the purpose of model evaluation. The model performance is assessed by computing four conventional statistical metrics: the correlation coefficient (R), normalized mean bias (NMB), normalized mean error (NME), and index of agreement (I), which are defined as follows:

$$R = \frac{\sum_{i=1}^N (p_i - \bar{p})(o_i - \bar{o})}{\sqrt{\sum_{i=1}^N (p_i - \bar{p})^2 \cdot \sum_{i=1}^N (o_i - \bar{o})^2}} \quad (1)$$

$$\text{NMB} = \frac{\sum_{i=1}^N (p_i - o_i)}{\sum_{i=1}^N o_i} \times 100\% \quad (2)$$

$$\text{NME} = \frac{\sum_{i=1}^N |p_i - o_i|}{\sum_{i=1}^N o_i} \quad (3)$$

$$I = 1 - \frac{\sum_{i=1}^N (p_i - o_i)^2}{\sum_{i=1}^N (|p_i - \bar{o}| + |o_i - \bar{o}|)^2}, \quad (4)$$

where p_i , o_i , and N represent model predicted data, observational data, and the number of data pairs, respectively. Equation (4) indicates that I is a positive value no greater than 1, the larger the value of I , the better the model performs, and a value of 1 indicates a perfect match between the model and observations.

2.2 Scenarios of urban land expansion

This work investigates the sensitivity of climatic conditions and atmospheric chemical fields to changes in urban land cover on a regional scale. Four idealized urban land surface expansion scenarios are designed within the WRF/Chem modeling framework by modifying certain static geographical parameters. The land-use fraction by category describes the percentage coverage of different land-use categories within a given grid cell, and the land-use index indicates the grid's dominant land-use category. The BASE run uses the prescribed 2008 IGBP MODIS 20-category land-use data. The GE0.2 run converts all cells with an urban land-use fraction of 0.2 or more to urban land-use index. The GE0.1 (urban land-use fraction ≥ 0.1) and GT0 (urban land-use fraction > 0) urban expansion scenarios are constructed similarly. Note that only the land-use index has been modified since the Noah land surface model considers only land-use index rather than a mosaic of multiple land-use categories with various land-use fractions for the version of WRF/Chem used in this study. Figure 1 shows a schematic map of the four idealized urban land expansion scenarios (i.e., BASE, GE0.2, GE0.1, and GT0). The urban land surface expands extensively over the Yangtze River Delta, and most newly urbanized regions aggregate around the periphery of the original urban districts. Figure S1 (in the Supplement) shows the original dominant land-use categories of newly urbanized cells in the GT0 run, as well as a contour map of terrain height in the domain of interest. Most new urban areas emerge to replace cropland, whereas few appear in mountainous areas.

2.3 Integrated process rate analysis

In Eulerian grid air quality models such as WRF/Chem and CMAQ, the numerical technique of operator splitting is used to solve the governing equations for species' concentrations. Operator splitting involves separating the continuity equation for each species into several simpler partial differential equations or ordinary differential equations consisting of one or two individual processes (Gipson, 1999). The technique of integrated process rate (IPR) analysis has been developed to track the accumulated contributions of individual physical and chemical processes to model predictions during run-time. IPR has already been fully implemented in CMAQ, and recent studies have reported its use in investigating a high ozone episode in the Yangtze River Delta (Li et al., 2012) and the Pearl River Delta (Wang et al., 2010), China, as well as the fate of major airborne pollutants in the southeastern US (Yang and Shiang-Yuh, 2013).

However, IPR has not yet been officially adopted in the WRF/Chem modeling framework. Jiang et al. (2012) added a simple process analysis scheme to WRF/Chem to calculate the contribution of photochemical and physical processes to O_3 evolution. In this paper, we extend this work by implementing an improved online IPR scheme in WRF/Chem to track contributions from 10 processes, namely horizontal and vertical advection (ADVH and ADVZ), emissions (EMISS), dry deposition (DRYDEP), turbulent diffusion (DIFF), convection (CONV), gas-phase chemistry (CHEM), cloud chemistry (CLDCHEM), aerosol processes (AERCHEM), and wet scavenging (WETSCAV). The calculation of dry deposition is based on resistance models for gaseous species (Wesely, 1989) and particles (Ackermann et al., 1998). Note Zhang and He (2014) recently developed a new algorithm that linked dry deposition of particles with canopies via leaf area index (LAI), which is not included in the version of WRF/Chem used in this study. Cloud chemistry refers to aqueous-phase processes in different types of clouds, and aerosol processes refer to microphysical nucleation, condensation, and coagulation, as well as the mass transfer between the gas phase and condensed phase. Convection refers to the subgrid convective transport and the scavenging within the wet convective updrafts, whereas wet scavenging refers to the both in-cloud rainout and below-cloud washout during large-scale precipitation. In the modal aerosol scheme MADE/SORGAM (Ackermann et al., 1998; Schell et al., 2001), $\text{PM}_{2.5}$ comprises Aitken- and accumulation-mode particles of sulfate, nitrate, ammonium, organic carbon (including SOA), and black carbon. The process contribution is calculated as the difference of the species' burden in each cell before and after each simulated process. In WRF/Chem, dry deposition is intermingled with vertical diffusion, so changes in the column burden during vertical mixing can be attributed to dry deposition. The IPR technique is verified by comparing the changes in species burden with the sum of contributions from the 10

processes mentioned above during each model output interval. As shown in Fig. S2, the net contribution of these 10 processes broadly matches the species concentration change.

3 Model evaluation

Figure 2 compares simulated versus observed daily mean surface concentrations of O₃, CO, and PM_{2.5} over five monitoring sites: NJ_ZHN (July 2012), NJ_XL (July 2012), SH_PD (September 2009), HZ_YH (April 2008), and HZ_JD (April 2008). The comparison indicates that WRF/Chem is capable of capturing the daily mean concentrations of surface O₃ ($R = 0.66$; $NME = 27\%$), CO ($R = 0.74$; $NME = 41\%$), and PM_{2.5} ($R = 0.63$; $NME = 29\%$). Recent evaluation of the ensemble of regional air quality models in the Air Quality Model Evaluation International Initiative (AQMEII) indicated that modeling of PM_{2.5} suffered from too low variability and underestimation (Im et al., 2015; Solazzo et al., 2012). However, in this study the daily mean observed and modeled PM_{2.5} concentrations in NJ sites are 47.4 ± 22.7 and $51.3 \pm 29.0 \mu\text{g m}^{-3}$, while in the SH_PD site, they are 41.8 ± 12.3 and $44.1 \pm 21.0 \mu\text{g m}^{-3}$, respectively. Both the mean and daily variability (indicated by the ratio of the standard deviation of the measurements to the standard deviation of the model) of PM_{2.5} concentrations are overestimated a bit. WRF/Chem generally captures the diurnal variation of surface O₃ well, (i.e., $R = 0.74$, $NMB = 6.7\%$, $NME = 34.1\%$, and $I = 0.86$). The model also reproduces the hourly surface burden of PM_{2.5} and CO, with NMEs of 63.4 and 52.6%, respectively. In addition, WRF/Chem captures the monthly mean surface concentrations of O₃, CO, and PM_{2.5} fairly well (although O₃ in SH is over-predicted by 17% and CO in NJ is under-predicted by 30%). A number of previous air quality studies have evaluated the performance of WRF/Chem in simulating a range of chemical species (e.g., PM_{2.5}, CO, and O₃) over China (Li et al., 2012; Tie et al., 2007, 2013), and these have reported similar results.

4 Impacts of urban land expansion on regional atmospheric environment

4.1 Urbanization-induced concentration changes

Urban land expansion significantly alters the local synoptic conditions (see Fig. S3 in the Supplement), e.g., an increase in 2 m temperature and boundary layer height, and a decrease in 2 m relative humidity and 10-m wind speed (this could be different for regions where urban land cover replaces forests). Changes in meteorology impact ambient air quality, even when anthropogenic emissions remain constant. We focus on the response of two gaseous species (i.e., CO and O₃) and two aerosol species (i.e., EC and PM_{2.5}). EC and CO are used to study how urban land expansion would impact the dispersion and dilution of primary pollutants. EC

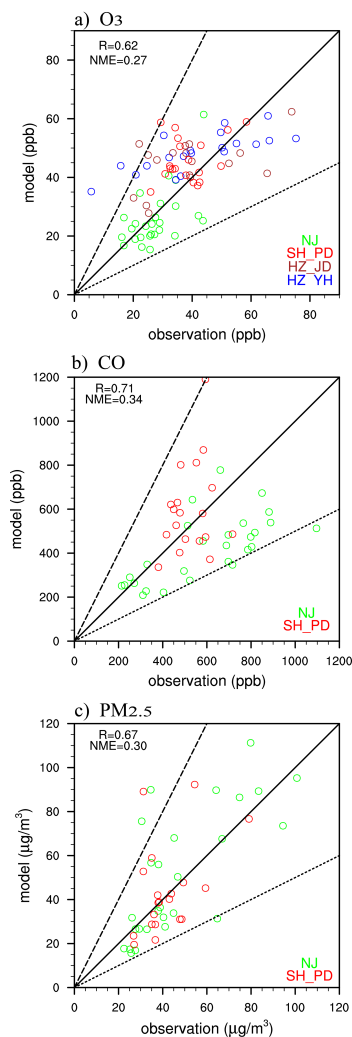


Figure 2. Modeled versus observed daily mean surface concentrations of (a) O₃, (b) CO, and (c) PM_{2.5} at NJ (July 2012), SH_PD (September 2009), HZ_YH (April 2008), and HZ_JD (April 2008). The solid line indicates the 1 : 1 line; dashed lines indicate the 1 : 2 and 2 : 1 lines.

includes Aitken-mode EC (ECI) and accumulation-mode EC (ECJ), and the aerosol scheme simulates the aging process by converting ECI to ECJ. O₃ and PM_{2.5} are used to further investigate the effects of urban land expansion on secondary pollutants.

The model surface layer (Fig. 3) and 800 hPa layer (Fig. 4) are selected to study the 5-year mean concentrations in July of CO, EC, O₃, and PM_{2.5} in the four urbanization scenarios. In the BASE run, high levels of surface CO (~ 850 – 1250 ppb), EC (~ 9 – $13 \mu\text{g m}^{-3}$), and PM_{2.5} (~ 90 – $130 \mu\text{g m}^{-3}$) are found only in urban areas where anthropogenic emissions are high. In contrast, terrestrial O₃ (~ 24 – 32 ppb) is more evenly distributed on the regional scale. At 800 hPa, concentrations of CO (~ 40 – 70 ppb), EC (~ 0.2 – $0.4 \mu\text{g m}^{-3}$), O₃ (~ 24 – 30 ppb), and PM_{2.5} (~ 10 –

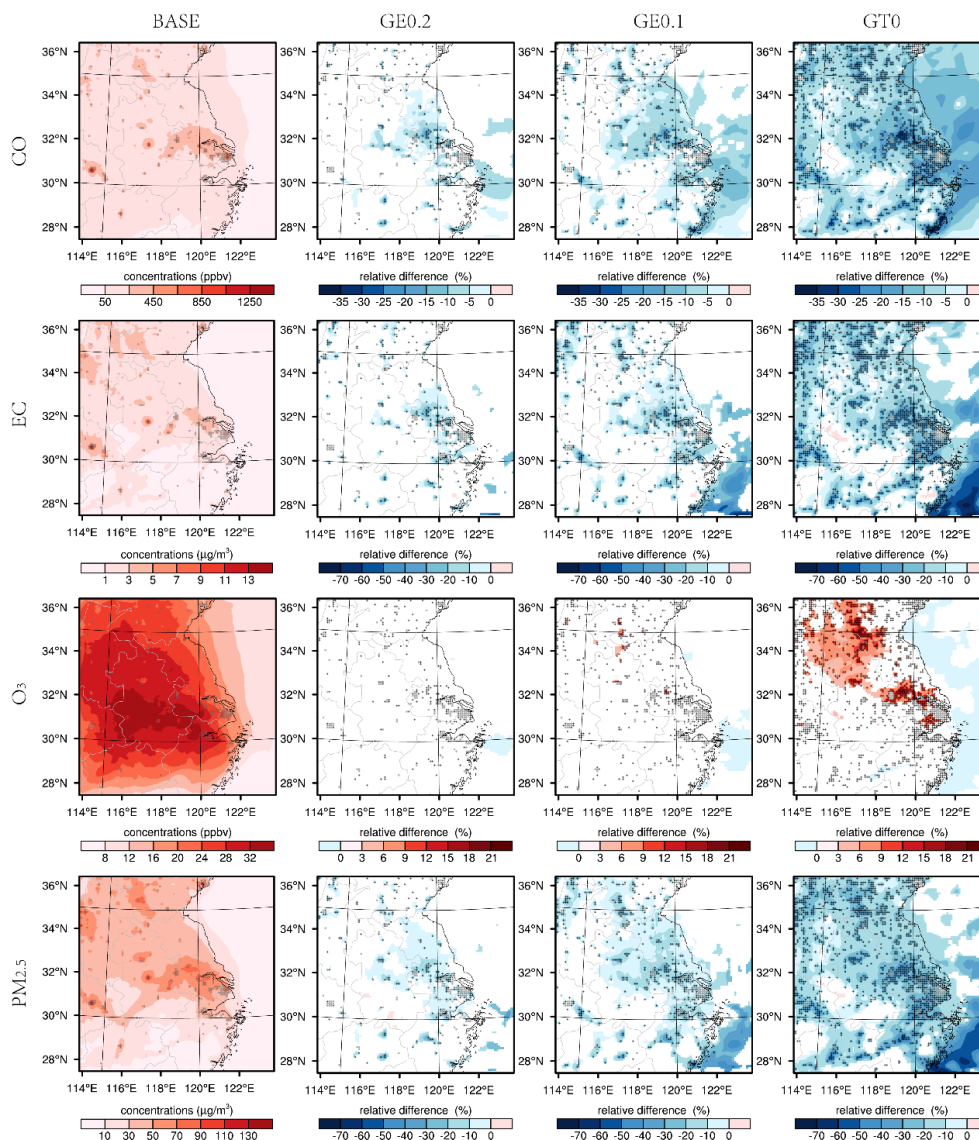


Figure 3. Five-year mean surface concentrations in July of CO, EC, O₃, and PM_{2.5} in the BASE run (left), and the relative difference (only cells exceeding the 95 % significance level are shown) of each urban land expansion scenario relative to BASE (right three columns). Gray circles indicate urban areas in the BASE run; black crosses indicate newly urbanized cells in GE0.2, GE0.1, and GT0.

$20 \mu\text{g m}^{-3}$) over the North China Plain appear much higher than those in the southern domain, consistent with the satellite-observed pollution distribution features over this domain (e.g., Liu et al., 2013). A one-tailed student t test (based on the standard error computed from hourly variability) is used to determine whether the assumed expansion of urban land causes changes in local monthly mean concentrations that are significant at the 95 % confidence level. In the surface layer, the change in dominant land-use type to urban generally induces a significant decrease in surface concentrations of CO (up to -44% ; domain-wide average of -11% , or up to 40 ppb decrease in the GT0 run), EC (up to -80% ; domain-wide average of -21% , or $-0.3 \mu\text{g m}^{-3}$ in

the GT0 run), and PM_{2.5} (up to -74% ; domain-wide average of -21% , or $-5.4 \mu\text{g m}^{-3}$ in the GT0 run) in all urbanization scenarios. However, the changes in surface O₃ are generally insignificant in GE0.2. Urban land expansion leads to a moderate increase in surface O₃ (maximum of 22 %; domain-wide average of 0.3 %, equivalent to 0.1 ppb in the GT0 run) over the northern terrestrial domain in the GE0.1 and GT0 runs. At 800 hPa, the expansion of urban land significantly increases the local concentrations of CO (with a domain-wide average of 16 %, and up to 5.6 ppb in the GT0 run), EC (domain-wide average of 50 %, or $\sim 0.05 \mu\text{g m}^{-3}$ in the GT0 run), O₃ (domain-wide average of 16 %, or ~ 2.8 ppb in the GT0 run), and PM_{2.5} (domain-wide average of 65 %,

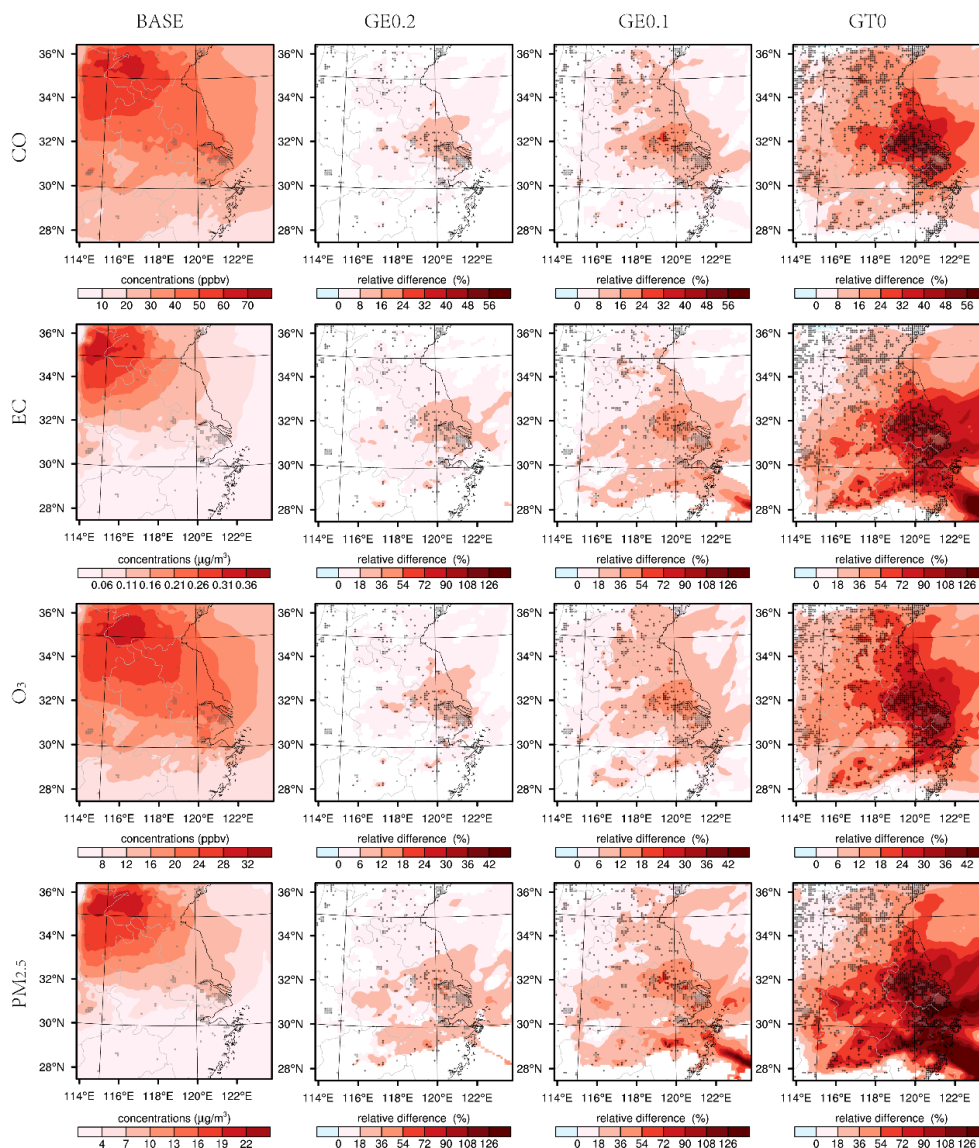


Figure 4. Same as Fig. 3, but at 800 hPa.

or $\sim 4.3 \mu\text{g m}^{-3}$ in the GT0 run) in the different urbanization scenarios. The effect of urban land expansion on CO, EC, O₃ and PM_{2.5} concentrations is consistent in each year, albeit with slight differences in magnitude (not shown).

4.2 Linearity of the urbanization–response relationship over east China

The urbanization–response relationship is a complex function of local synoptic conditions, large-scale circulation, land surface type, the physical and chemical properties of an airborne contaminant, and its emissions (e.g., release height, frequency, and amount), as well as the time scale being considered. The strength of urban land forcing (e.g., the sensitivity of an atmospheric variable to urban land expansion) can

be quantitatively evaluated as the perturbation of this variable from its base condition. Figure 5 shows the response of the 5-year mean concentrations in July of CO, EC, O₃, and PM_{2.5} to changes in domain-wide (i.e., east China) urban land coverage. At both the surface and 800 hPa, the response curves are nonlinear and the rate of domain-wide concentration changes decreases as more urban land emerges. However, as shown in Figs. 3 and 4, the concentration response is nonuniformly distributed, and becomes stronger when large tracts of new urban land appear. This indicates that the aggregation state (further discussed in the next paragraph) of newly urbanized areas would alter the strength of urban land forcing.

The forcing effect of urban land expansion on the spatial distribution of air pollutants is not usually limited to

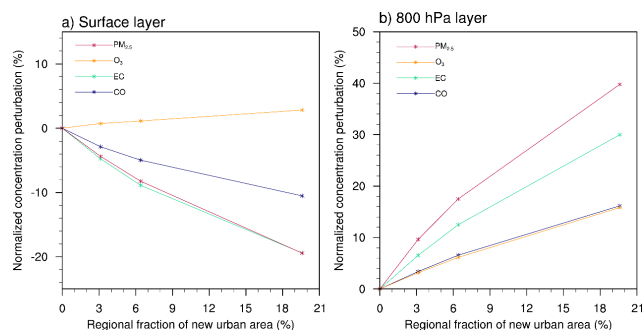


Figure 5. Normalized perturbations (relative to the BASE simulation) for three urbanization scenarios of the 5-year mean concentrations in July of CO, EC, O₃, and PM_{2.5} at the (a) surface and at (b) 800 hPa. Values are averaged over land for the entire domain. Corresponding domain-wide land fraction of new urban areas are 3, 6, and 20 %, respectively, relative to BASE.

newly urbanized areas, but has a distance of extended influence. To differentiate the shape of urbanization–response curves at different locations, we use LOCAL to denote these newly urbanized cells, and ADJACENT to represent the non-urbanized cells neighboring LOCAL. We further define an aggregation parameter (Agg) for a given LOCAL cell as the number of the surrounding cells that are also LOCAL; we limit the number of surrounding grid cells for this analysis to $5 \times 5 - 1$ or 24 cells (2400 km^2). The “local” or “adjacent” forcing is defined as

$$f_j = \frac{\sum_{i=1}^{N_j} \frac{VC_i}{VB_i}}{N_j}, \quad (5)$$

where f_1 (i.e., $j = 1$) denotes local forcing (LF), N_1 is the number of domain-wide LOCAL cells, and VC_i and VB_i denote the values of a certain atmospheric variable in cell i of the perturbation run and the BASE run, respectively. f_2 denotes adjacent forcing (AF) over the ADJACENT cells, and N_2 is the number of domain-wide ADJACENT cells.

Figure 6 illustrates the LF and AF induced by urban land expansion (i.e., the perturbation of a 5-year mean in July concentrations of CO, EC, O₃, and PM_{2.5} from the BASE situation) in all three idealized urbanization scenarios. At the surface, the relationship between LF and Agg is nearly linear. Each 10 % increase in Agg is associated with a 1.6, 1.8, and 2.2 % decrease in LOCAL CO, EC, and PM_{2.5} concentrations, respectively, and a 1 % increase in O₃ concentrations. The AF–Agg curves are similar to those for LF–Agg, but have weaker responses. The linearity can be explained as follows: with increasing Agg, there are more LOCAL cells near a given cell, so the same number of adjacent effects are added to the given cell. At 800 hPa, changes in the contaminant burden seem to be more sensitive to the aggregation level of newly urbanized cells than at the surface, and particles seem to be more susceptible than gases. The associ-

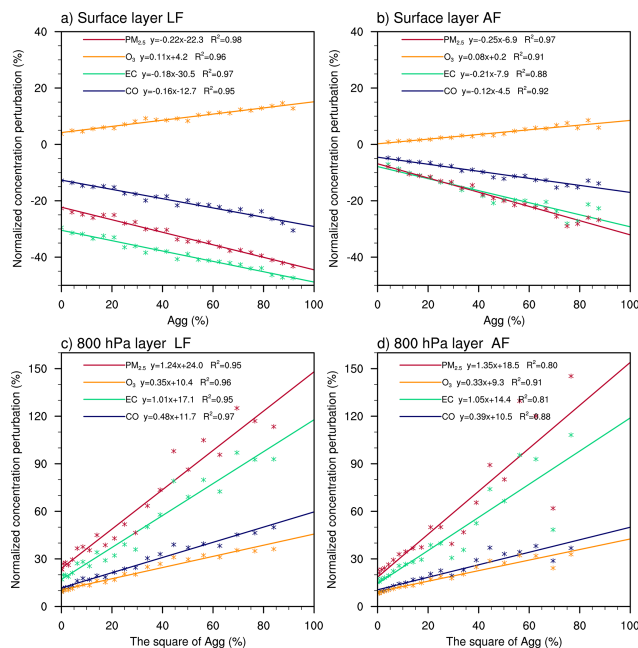


Figure 6. Relationship between normalized perturbations of 5-year mean July concentrations of CO, EC, O₃, and PM_{2.5} and Agg at the surface (top), and the square of Agg at 800 hPa (bottom) for the LOCAL forcing (LF, left) and ADJACENT forcing (AF, right). Agg is defined as the occupation rate of the newly urbanized cells to the surrounding 24 ($5 \times 5 - 1$) cells. Linear regression results are also shown.

ated urbanization–response curves become nonlinear. It can be observed that both LF and AF are linearly associated with the square of Agg, which means each 10 % increase in the square of Agg may enhance air pollution concentrations by about 5–10 % at 800 hPa, with the maximum sensitivity for PM_{2.5} (12 %). This indicates that dense urbanization over east China may have a moderate dilution effect on surface air pollution, but could intensify pollutants aloft and therefore severe haze (i.e., visibility degradation) and ozone pollution if local emissions are not reduced in the future.

Besides the response of air pollutants, the perturbations in July-mean boundary layer height, 2 m temperature, and 2 m relative humidity also increase linearly with Agg ($R^2 > 0.96$, shown in Fig. S4 in the Supplement). These results indicate that when large tracts of new urban land emerge, impacts of land-cover change on meteorology and air pollutant concentrations can be magnified.

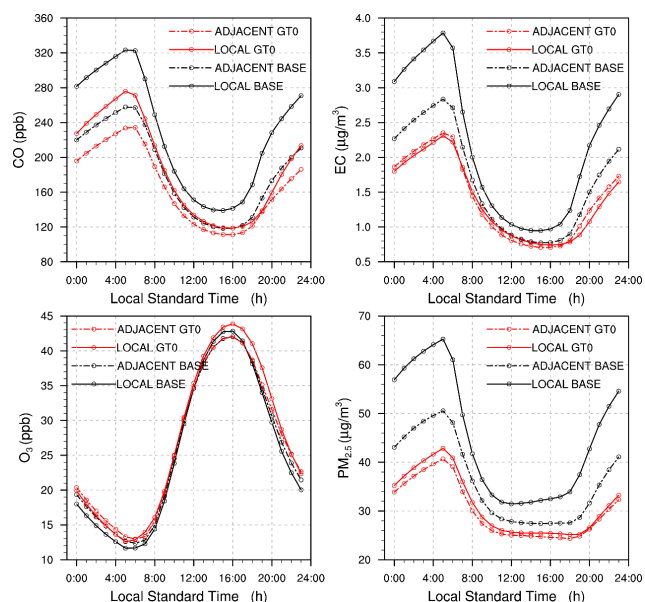


Figure 7. Simulated 5-year mean July diurnal cycle of CO, EC, O₃, and PM_{2.5} at the surface, averaged over domain-wide LOCAL cells (solid lines) and ADJACENT cells (dashed lines).

5 Mechanism governing the urbanization–response relationship

5.1 Process contribution to surface air quality changes

Figure 7 shows the 5-year mean in July diurnal cycles of CO, EC, O₃, and PM_{2.5} surface concentrations averaged over the domain-wide LOCAL cells and the ADJACENT cells. At the surface, CO, EC, and PM_{2.5} share a diurnal variation pattern in which concentrations peak at dawn (~05:00 LST) and reach a trough in the late afternoon (~16:00 LST). Concentrations over LOCAL cells are usually higher than those over the ADJACENT regions, particularly during the night. However, for O₃, the opposite diurnal variation pattern can be observed, and the difference between LOCAL and ADJACENT cells is small. Urban land expansion leads to substantial changes in species concentrations, but has little effect on the shape of the diurnal cycle. As urban land expands, CO, EC, and PM_{2.5} tend to evolve toward lower burden levels. In contrast, when averaged over the domain, the increment in surface O₃ concentrations during most of the day is insignificant. Though the resulting concentration changes in LOCAL and ADJACENT are quite similar for these four species, the IPR analysis suggests that the underlying mechanisms that drive the forcing–response relationship are different.

Figure 8 illustrates the 5-year mean in July diurnal cycles of IPR contributions in the BASE run and their deviations in the GT0 run over the domain-wide surface LOCAL cells and ADJACENT cells. The daytime period is chosen as 07:00–18:00 LST, with the rest of the day considered to be nighttime. In the BASE run, emissions are the dominant

source of CO over the LOCAL cells, and the dominant sink is turbulent transport (daytime advection is also a contributing sink). EC follows a similar IPR pattern to CO, except that dry deposition is also a major sink, accounting for about 40 % of the total EC removal. Since this study considers constant CO and EC emissions, diurnal variability in concentrations is dominated by variations in the strength of vertical transport. During the daytime, vertical transport is strong, and CO and EC are depleted at the surface. However, during the nighttime, vertical transport becomes weaker, which allows CO and EC to accumulate. The diurnal cycle of IPR for PM_{2.5} is very similar to that of EC, but aerosol processes play an important role. During the daytime, the source of PM_{2.5} is dominated by surface emissions, but the sinks are quite complicated, including turbulent diffusion (~41 %), dry deposition (~36 %), and aerosol processes (~23 %). Note that by conducting IPR analyses within CMAQ, Yang and Shiang-Yuh (2013) found that depletion in aerosol processes can act as a sink for PM_{2.5}. At night, the production of PM_{2.5} through aerosol processes forms 22 % of the source. The IPR diurnal cycle for O₃ is quite different. During the daytime, the major sources for surface O₃ are photochemical production (~37 %) and turbulent transport (~63 %), and the sink is overwhelmingly dry deposition. At night, removal of O₃ through gas-phase reactions and dry deposition accounts for 40 and 60 % of the sink, respectively. The diurnal cycles of IPR contribution over the ADJACENT cells are similar to those of LOCAL cells, except that vertical diffusion becomes a source for PM_{2.5} during the daytime, compensating for the strong loss by aerosol processes and dry deposition.

In the GT0 run, as urban land expands, changes in horizontal (vertical) advection tend to increase (reduce) the surface concentration of all four species over the LOCAL cells, whereas the opposite is true for the ADJACENT cells. The associated surface wind field perturbations due to urban land expansion are shown in Fig. 9. The urban land expansion could strengthen the southeasterly sea breeze over marine domain and near the east seaboard of China, due to the increased difference in thermal properties between land and sea (as the urban land is characterized with a greater heat capacity, thermal conductivity, and lower albedo). However, perturbation of wind field in the inner terrestrial is more complicated, generally speaking; the replacement of natural land by urban land would reduce the local pressure (up to 30 Pa) and form a cyclonic convergence zone. The divergence of the perturbed wind field can be calculated by a centered finite difference scheme with a one-sided difference boundary. Values of convergence up to $-6 \times 10^{-5} \text{ s}^{-1}$ can be observed in most of the newly urbanized areas, similar to the results of Bornstein and Lin (2000), who concluded that UHI would induce a convergence (with a magnitude of -10^{-5} s^{-1}) zone over Atlanta. Figure 10 shows the perturbed wind field in the three vertical–longitudinal cross sections of CS1, CS2, and CS3 mentioned in Fig. 1. The emergence of urban land induces local updrafts of $\sim 1 \text{ cm s}^{-1}$, which enhances the venti-

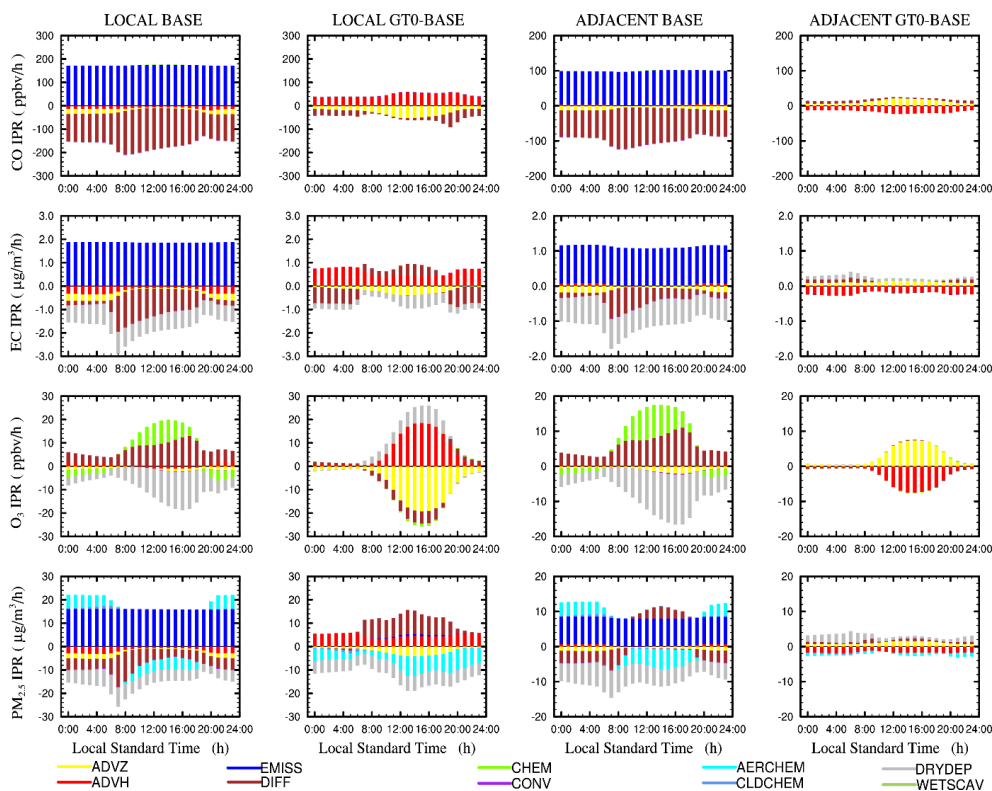


Figure 8. Five-year mean in July diurnal cycles of IPR for surface CO, EC, O₃, and PM_{2.5} concentrations. Values are averaged over all LOCAL (left two columns) and ADJACENT (right two columns) cells. Results are shown for the BASE simulation and for differences between GT0 and BASE.

lation of primary pollutants to the free troposphere; adjacent downdrafts are also observed. The perturbed wind induced by urban land expansion generally forms convergence zones above the LOCAL cells and divergence zones over the ADJACENT cells (Fig. 9). Urban heat island circulation (UHIC) is enhanced, which explains the changes in the contribution of advection.

The effects of urban land expansion are not limited to the UHIC-induced advection changes. In the surface layer, the vertical diffusion of CO is intensified over LOCAL cells (especially during the night). EC differs from CO in that the loss due to dry deposition markedly increases over the entire day, while the sink due to diffusion is only reduced during the daytime but is increased at night. The sum of dry deposition and turbulent diffusion reflects the role of vertical mixing in relocating the airborne pollutants vertically. The sink due to the vertical mixing of EC is intensified. It can be concluded that the enhanced advection and turbulent mixing in the vertical direction are the key factors in reducing the surface concentrations of CO and EC. For O₃, dry deposition, vertical diffusion, and daytime photochemical production and nighttime chemical depletion are all reduced at the surface, resulting in a net weak enhancement of surface O₃ averaged over domain-wide LOCAL cells. The dry deposition of O₃ is reduced because the canopy resistance in-

creases as vegetation is replaced by urban land; however, the dry deposition of particles is fostered by the intensified surface turbulence. Vertical diffusion is possibly hindered by convergent updrafts caused by UHIC, and the daytime photochemical production and nighttime chemical depletion are reduced because of the decreased abundance of precursors. For PM_{2.5}, daytime loss and nighttime production via aerosol processes are enhanced and hindered, respectively; this may be because the urbanization-induced decrease in precursor concentrations restrains gas-to-particle mass transfer. At the same time, dry deposition and vertical diffusion are also enhanced during the daytime. Therefore, the increased sink resulting from aerosol processes and dry deposition is the key factor reducing PM_{2.5} concentrations at the surface. Over the ADJACENT cells, urbanization-induced outward horizontal advection contributes to the lower burden of CO, EC, and PM_{2.5}, and the sink term due to vertical mixing decreases.

5.2 Urbanization-induced process-level vertical profile changes

Figure 11 shows the 5-year mean in July vertical profile of the four species averaged in the domain-wide LOCAL and ADJACENT cells of the BASE and GT0 runs. In both types of cells, CO, EC, and PM_{2.5} exhibit similar patterns; as ur-

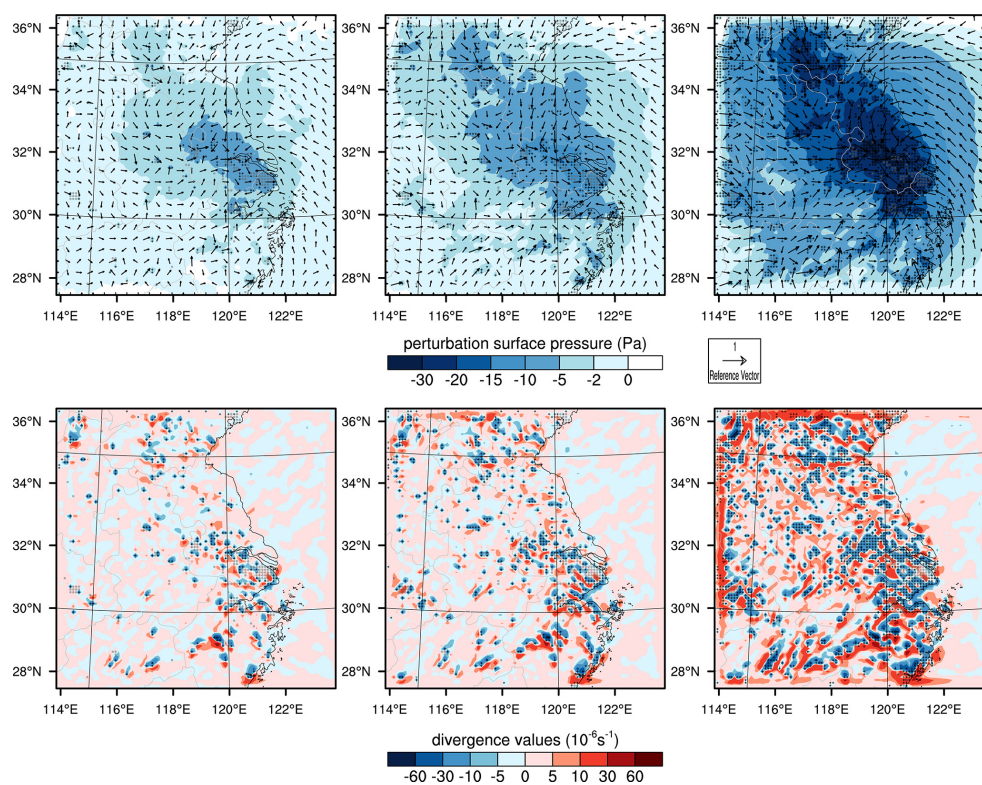


Figure 9. Five-year mean July perturbations of surface pressure and wind field (top three plots; reference velocity is 1 m s^{-1}) and the divergence of surface wind (bottom three plots) in GE0.2, GE0.1, and GT0 runs. Gray circles indicate the locations of urban cells in the BASE run; black crosses indicate the locations of newly urbanized areas in GE0.2, GE0.1, and GT0 runs.

ban land expands, the atmospheric burden decreases near the surface (below 1 km), but increases at higher altitudes (1–4 km). On the other hand, the concentration of O_3 increases at most heights from the surface to a height of about 4 km. Unlike near the surface, the magnitude of the concentration perturbations aloft (1–4 km) in both grids is commensurate.

Figure 12 illustrates the vertical profile of 5-year mean in July daytime and nighttime IPR contributions for CO, EC, O_3 , and $\text{PM}_{2.5}$ in the BASE and GT0 runs, averaged over all LOCAL cells. Convective scavenging generally plays a minor role in removing these four species. For CO and EC, vertical mixing and advection play key roles in constraining the vertical profiles, and the net diffusion is unidirectional from the ground to higher altitudes. The extent of vertical transport during the daytime is higher than that during nighttime. The forcing of urban land expansion on the transport of primary pollutants is characterized by UHIC-induced advection changes and enhanced vertical mixing, leading to the decreased vertical concentration gradient (as shown in Fig. 11). A positive perturbation in the horizontal advection contribution and a negative perturbation in the vertical advection contribution are found in the lower atmosphere (below 500 m), whereas the opposite is true in the upper atmosphere (~ 0.5 –3 km). For CO and EC (only during nighttime), the enhanced sink and source due to vertical mixing in lower and upper at-

mosphere, respectively, could be the key reasons for changes of vertical profile, and advection appears to compensate and balance this effect. However, for EC above 1 km, as surface dry deposition is strengthened markedly in the daytime, diffusion from the lower atmosphere is dampened; this is compensated for by the enhanced upward advection.

For O_3 , advection, vertical mixing, and gas-phase reactions all play important roles in constraining its vertical profile. Though UHIC-induced horizontal and vertical advection changes cause the IPR to shift significantly across all layers, net advection is not the key process driving the changes in the vertical O_3 profile. Near the ground level, the expansion of urban land fosters upward diffusion and hinders downward diffusion to the surface layer. O_3 production is determined by the availability of precursors, which is increased in the 1–3 km zone by the enhanced uplifting of primary pollutants. The dampened dry deposition and enhanced daytime photochemical production (at around 0.5–3 km) are responsible for a higher O_3 profile.

Besides the transport of precursors, other meteorological factors may also influence O_3 production. The bottom three plots in Fig. 10 show the distribution of chemical production (ppb h^{-1}), cloud water, and air temperature differences (GT0 minus BASE during the period 12:00–17:00 LST) in the cross sections of CS1, CS2, and CS3 (defined in Fig. 1). As

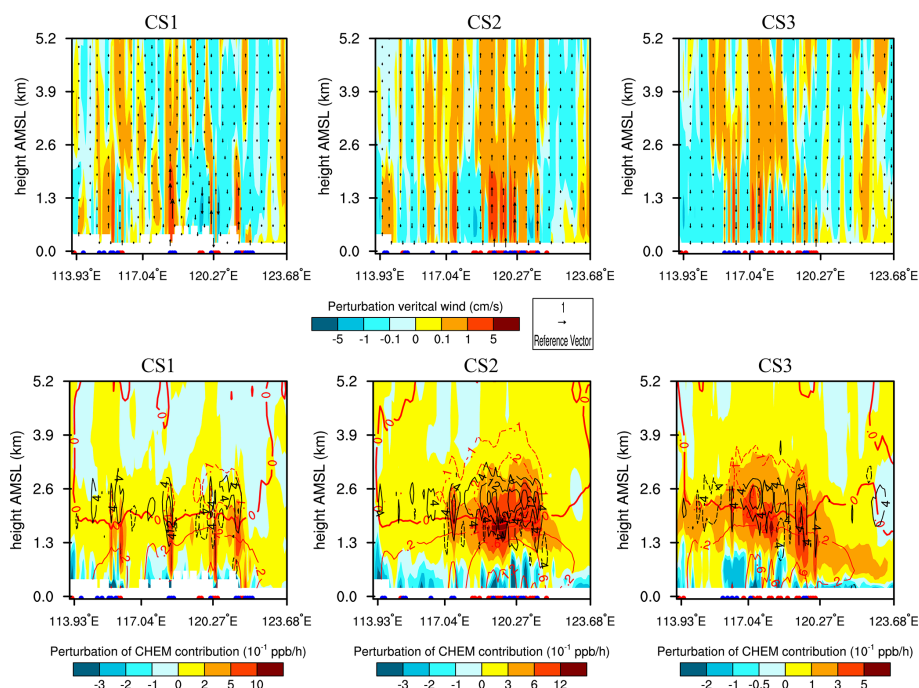


Figure 10. Distribution of 5-year mean July perturbations (GT0 minus BASE) of vertical wind velocities (top three plots; reference wind velocity is 1 cm s^{-1}), O_3 production (color, ppb h^{-1}), cloud water content (black line, mg kg^{-1}), and air temperature (red line, K) during 12:00–17:00 LST (bottom three plots) in CS1, CS2, and CS3. Red and blue dots indicate the longitudes of LOCAL cells in the GT0 run along the cross-section lines and adjacent areas, respectively.

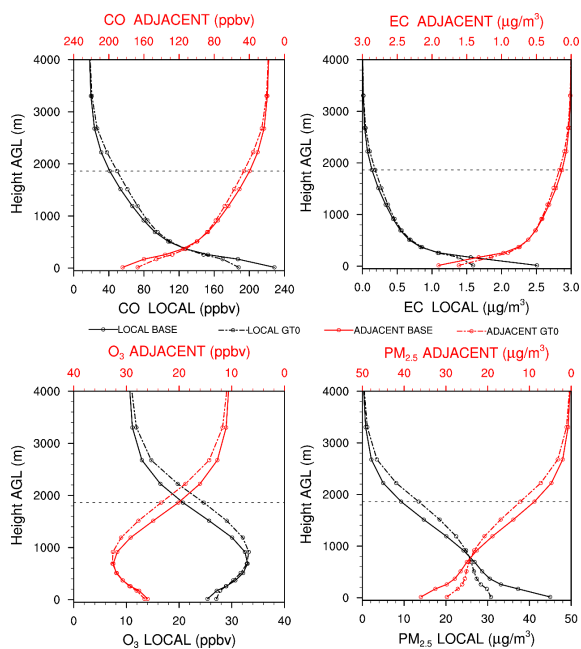


Figure 11. Five-year mean July vertical profiles of CO, EC, O_3 , and $\text{PM}_{2.5}$ concentrations over the LOCAL cells (black) and ADJACENT cells (red) in the BASE (solid lines) and GT0 run (dashed lines). The horizontal dashed lines indicate the height of 800 hPa.

urban land expands, air temperatures increase (up to 1.2°C) in the lower layers (below 0.5 km), but decrease slightly above 2 km. However, photochemical production of O_3 is intensified only at altitudes higher than 2 km. This indicates that changes in air temperature may not be the principal factor determining O_3 production above the PBL. As shown in Fig. 10, the locations of newly urbanized cells exactly match the zones where photochemical production of O_3 is reduced in lower layers, but cloud water content is significantly increased above 1 km. Low altitude clouds efficiently scatter shortwave radiation, thus hindering photochemical reactions below clouds; thus, urban land forcing indirectly effects the spatial distribution of O_3 .

As shown in Fig. 12, aerosol chemistry, vertical mixing, and advection all contribute strongly to constraining the $\text{PM}_{2.5}$ vertical profile, with wet scavenging and cloud chemistry playing relatively minor roles. During the daytime, the contribution of aerosol chemistry is negative near the surface, but turns positive at higher altitudes. At night, the contribution of aerosol chemistry remains positive in all vertical layers. The net vertical turbulent transport is upward in the surface layer, but reverses to downward above 0.5 km. Similar to O_3 , as urban land expands, changes in the vertical profiles of precursors result in enhanced aerosol production at 0.5–3 km, and enhanced loss below 0.5 km (where the downward diffusion is intensified). The perturbation of dry deposition and aerosol processes largely explains the $\text{PM}_{2.5}$

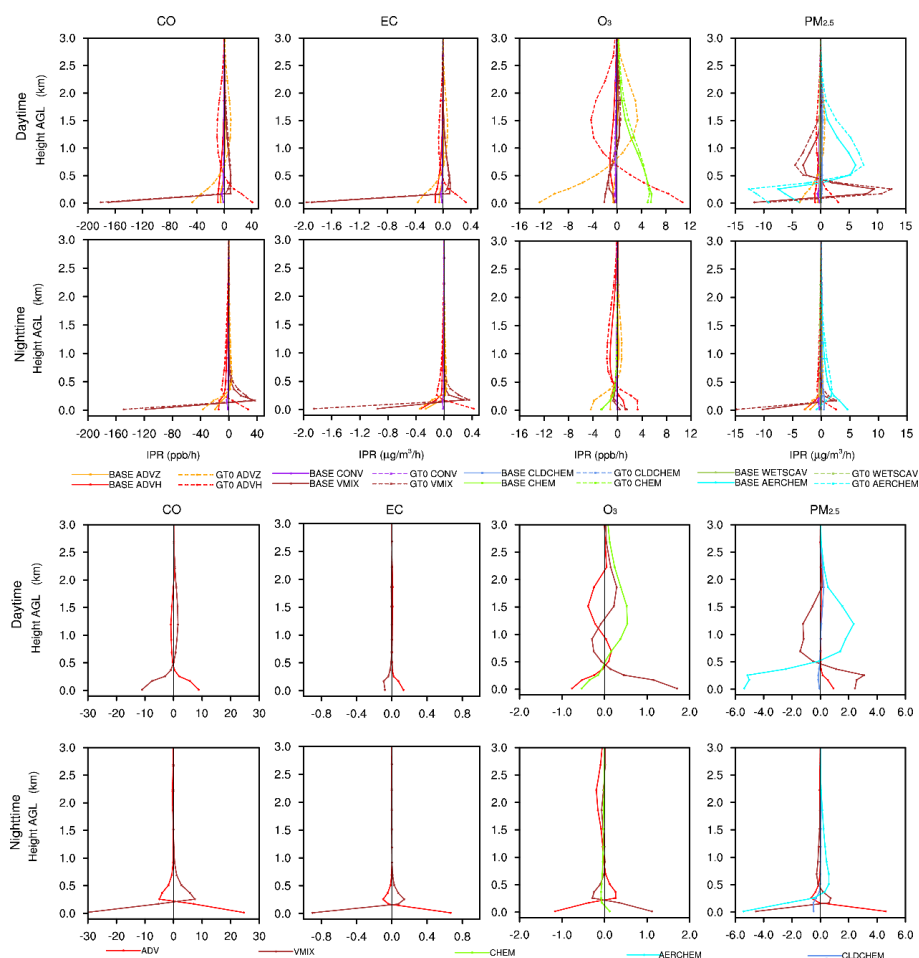


Figure 12. Five-year mean in July vertical profiles of diurnal (07:00–18:00 LST) and nocturnal (19:00–06:00 LST) IPR for CO, EC, O₃, and PM_{2.5} concentrations in the BASE and GT0 run (top eight figures). The bottom eight plots show the difference in IPR between GT0 and the BASE simulation averaged over domain-wide LOCAL cells.

vertical profile changes. Alike the case for the photochemical formation of O₃, the formation of PM_{2.5} through gas-phase/particle partitioning and cloud chemistry is also influenced by the relocation of humidity, as simulated by the MADE/SORGAM scheme (please refer to the Supplement for details). As shown in Fig. S5 in the Supplement, the production of PM_{2.5} through cloud chemistry increase (decrease) exactly where the humidity increases (decreases).

The caveats of this study are as follows. (1) The forcing of urban land expansion on the atmospheric environment is confined to the regional scale. Feedback between mesoscale circulation and large-scale circulation, as well as inflows of airborne pollutants from outside the domain of interest, has been ignored. (2) It is important to note that emissions are assumed to remain constant during our study time period. We chose constant emissions to ensure we could tease out the effects of land-cover-induced changes on air quality without confounding changes in emissions. Sensitivity experiments show that at the surface, the diluting effects of ur-

ban land could be offset, only if the emission augment is high enough for CO (~40%) and EC (~100%) in LOCAL cells (see Figs. S6–S8 in the Supplement for details). (3) The BULK urban canopy scheme used in this work does not resolve the urban morphology, and therefore cannot further investigate how urban canopy parameters, such as the building height and anthropogenic heat, would impact the climatic conditions and air quality. The urbanization–response relationship unveiled in this work could be urban scheme-dependent. In future studies, we will focus on addressing these effects to better quantify the urbanization–response relationship, which could provide support to urban planning.

6 Conclusions

We have used an online coupled mesoscale meteorology–chemistry model (WRF/Chem) with BULK urban scheme embodied in Noah land surface model and an improved integrated process rate (IPR) analysis scheme to study the effects

of urban land expansion in eastern China on climate and air quality during the month of July. Urban land expansion could significantly alter local synoptic conditions (e.g., increases in 2 m air temperature and boundary layer height and decreases in 2 m relative humidity). Above the newly urbanized grid cells (referred to as LOCAL cells), horizontal perturbations in wind form cyclonic convergence ($\sim 10^{-5} \text{ s}^{-1}$) zones, and vertical perturbations in wind lead to updraft flows ($\sim 1 \text{ cm s}^{-1}$). This urbanization-induced circulation consequently impacts ambient air quality, even when surface emissions remain constant. For primary pollutants with strong surface emissions (e.g., CO and EC), urban land expansion causes concentrations to decrease below 500 m but increase significantly between 1 and 3 km. On the other hand, the O_3 burden averaged over LOCAL cells consistently increases from the surface to about 4 km. For $\text{PM}_{2.5}$, though its source includes both primary emissions and secondary formation, the changes in vertical profile caused by urban land expansion are consistent with those of CO and EC.

The effects of urban land expansion are not localized, but rather its influence extends to neighboring areas. In this study, the local forcing (LF) was found to be significantly larger than adjacent forcing (AF) at the surface, especially for particulate matter. The aggregation state of newly urbanized areas plays an important role in determining the strength of LF and AF. We found that perturbations of CO, EC, O_3 , and $\text{PM}_{2.5}$ change linearly with the aggregation parameter (Agg) at the surface, and with the square of Agg at 800 hPa ($R^2 > 0.94$). In addition, the perturbations of mean July levels of boundary layer height, 2 m temperature, and 2 m relative humidity increase linearly with Agg ($R^2 > 0.96$). This result indicates that when large tracts of new urban land emerge, the effects of urban expansion on atmospheric physics and chemistry are magnified.

IPR was utilized to investigate the forcing mechanisms exerted by urban land expansion on the spatial distribution of CO, EC, O_3 , and $\text{PM}_{2.5}$ over the LOCAL cells. At the surface, a common feature of all four species is that they are governed by the UHIC effect, whereby horizontal advection causes increases in concentrations and vertical advection causes decreases in concentrations. Additionally, when nat-

ural vegetation was replaced by urban land, the sink term from dry deposition increased for particles but decreased for gaseous species. For primary pollutants CO and EC, enhanced advection and turbulent mixing in the vertical direction are the key factors in reducing the surface concentrations. On the other hand, for $\text{PM}_{2.5}$, increased sinks due to aerosol processes and dry deposition are the key factors in reducing surface concentrations. For O_3 , the reduced dry deposition and vertical diffusion, as well as the relocation of precursors, played an important role in constraining the surface concentration, resulting in a net enhancement of the surface O_3 averaged over all LOCAL cells.

In contrast to the surface conditions, urban land expansion may induce substantial increases in air pollution at higher altitudes. The positive contribution of vertical advection and the negative contribution of horizontal advection were found to be important in the build-up of air pollution in the upper atmosphere (0.5–3 km). For primary pollutants CO and EC (only during nighttime), the enhanced uplifting caused by strengthened turbulent diffusion (induced by urban land expansion) is the key factor leading to higher burdens in the upper atmosphere. However, in daytime, diffusion of EC from the lower atmosphere is dampened due to intensified dry deposition, which partially counters the concentration increases from enhanced upward advection. However, for secondary species, O_3 and $\text{PM}_{2.5}$, the relocation of precursors accelerates daytime chemical production in the upper atmosphere, which is the key factor in the higher burden of secondary pollutants at a height of about 1–4 km.

The above analysis has revealed the non-negligible and unique role of urban land forcing in impacting the advection, turbulent mixing, and dry/wet removal of pollutants, and indicated that dense urbanization has a moderate dilution effect on surface primary airborne contaminants, but may intensify severe haze and ozone pollution if local emissions are not well controlled. Further studies should simultaneously consider changes in both the land use (using a more complicated and advanced urban canopy scheme) and emission to better evaluate the potential environmental influence of any urbanization campaign.

Appendix A

Table A1. List of acronyms used in this work.

Acronyms	Description
LOCAL cells	the newly urbanized cells in each urban expansion scenario
ADJACENT cells	non-urbanized cells neighboring the LOCAL cells
ADVH	horizontal advection
ADVZ	vertical advection
ADV	the sum of horizontal and vertical advection
EMISS	emissions
DRYDEP	dry deposition
DIFF	turbulent diffusion
VMIX	the sum of dry deposition and turbulent diffusion
CONV	convective transport and scavenging
CHEM	gas-phase chemistry
CLDCHEM	cloud chemistry
AERCHEM	aerosol chemical and microphysical process
WETSCAV	wet scavenging by grid-scale precipitation

The Supplement related to this article is available online at doi:10.5194/acp-15-8597-2015-supplement.

Acknowledgements. We thank three anonymous reviewers for their thoughtful comments and helpful suggestions. This work was supported by funding from the National Natural Science Foundation of China under awards 41222011, 41390240, and 41130754, the Research Project of the Chinese Ministry of Education No. 113001A, the “863” Hi-Tech R&D Program of China under grant no. 2012AA063303, and the 111 Project (B14001).

Edited by: F. Dentener

References

- Ackermann, I. J., Hass, H., Memmesheimer, M., Ebel, A., Binkowski, F. S., and Shankar, U.: Modal aerosol dynamics model for Europe: Development and first applications, *Atmos. Environ.*, 32, 2981–2999, 1998.
- Arnfield, A. J.: Two decades of urban climate research: a review of turbulence, exchanges of energy and water, and the urban heat island, *Int. J. Climatol.*, 23, 1–26, 2003.
- Britter, R. and Hanna, S.: Flow and dispersion in urban areas, *Annu. Rev. Fluid Mech.*, 35, 469–496, 2003.
- Changnon, S. A.: Inadvertent weather modification in urban areas: Lessons for global climate change, *B. Am. Meteorol. Soc.*, 73, 619–627, 1992.
- Chen, F. and Dudhia, J.: Coupling an advanced land surface-hydrology model with the Penn State-NCAR MM5 modeling system. Part I: Model implementation and sensitivity, *Mon. Weather Rev.*, 129, 569–585, 2001.
- Chen, F., Kusaka, H., Bornstein, R., Ching, J., Grimmond, C. S. B., Grossman-Clarke, S., Loridan, T., Manning, K. W., Martilli, A., Miao, S. G., Sailor, D., Salamanca, F. P., Taha, H., Tewari, M., Wang, X. M., Wyszogrodzki, A. A., and Zhang, C. L.: The integrated WRF/urban modelling system: development, evaluation, and applications to urban environmental problems, *Int. J. Climatol.*, 31, 273–288, doi:10.1002/joc.2158, 2011.
- Civerolo, K., Hogrefe, C., Lynn, B., Rosenthal, J., Ku, J. Y., Solecki, W., Cox, J., Small, C., Rosenzweig, C., Goldberg, R., Knowlton, K., and Kinney, P.: Estimating the effects of increased urbanization on surface meteorology and ozone concentrations in the New York City metropolitan region, *Atmos. Environ.*, 41, 1803–1818, doi:10.1016/j.atmosenv.2006.10.076, 2007.
- Coceal, O. and Belcher, S.: A canopy model of mean winds through urban areas, *Q. J. Roy. Meteor. Soc.*, 130, 1349–1372, 2004.
- Cui, Y. Y. and de Foy, B.: Seasonal Variations of the Urban Heat Island at the Surface and the Near-Surface and Reductions due to Urban Vegetation in Mexico City, *J. Appl. Meteorol. Clim.*, 51, 855–868, doi:10.1175/jamc-d-11-0104.1, 2012.
- De Meij, A., Bossioli, E., Penard, C., Vinuesa, J., and Price, I.: The effect of SRTM and Corine Land Cover data on calculated gas and PM₁₀ concentrations in WRF-Chem, *Atmos. Environ.*, 101, 177–193, 2015.
- Di Sabatino, S., Solazzo, E., Paradisi, P., and Britter, R.: A simple model for spatially-averaged wind profiles within and above an urban canopy, *Bound.-Lay. Meteorol.*, 127, 131–151, 2008.
- Fan, H. and Sailor, D. J.: Modeling the impacts of anthropogenic heating on the urban climate of Philadelphia: a comparison of implementations in two PBL schemes, *Atmos. Environ.*, 39, 73–84, 2005.
- Fernando, H., Lee, S., Anderson, J., Princevac, M., Pardyjak, E., and Grossman-Clarke, S.: Urban fluid mechanics: air circulation and contaminant dispersion in cities, *Environ. Fluid Mech.*, 1, 107–164, 2001.
- Fisher, B., Kukkonen, J., Piringer, M., Rotach, M. W., and Schatzmann, M.: Meteorology applied to urban air pollution problems: concepts from COST 715, *Atmos. Chem. Phys.*, 6, 555–564, doi:10.5194/acp-6-555-2006, 2006.
- Gipson, G. L.: Science algorithms of the EPA Models-3 community multiscale air quality (CMAQ) modeling system: process analysis, 37 pp., 1999.
- Grell, G. A., Peckham, S. E., Schmitz, R., McKeen, S. A., Frost, G., Skamarock, W. C., and Eder, B.: Fully coupled “online” chemistry within the WRF model, *Atmos. Environ.*, 39, 6957–6975, doi:10.1016/j.atmosenv.2005.04.027, 2005.
- Guenther, A., Karl, T., Harley, P., Wiedinmyer, C., Palmer, P. I., and Geron, C.: Estimates of global terrestrial isoprene emissions using MEGAN (Model of Emissions of Gases and Aerosols from Nature), *Atmos. Chem. Phys.*, 6, 3181–3210, doi:10.5194/acp-6-3181-2006, 2006.
- Harman, I. N., Barlow, J. F., and Belcher, S. E.: Scalar fluxes from urban street canyons part II: model, *Bound.-Lay. Meteorol.*, 113, 387–410, 2004.
- Heilig, G. K.: World Urbanization Prospects: The 2011 Revision, United Nations, Washington, D.C., 2012.
- Hong, S.-Y., Noh, Y., and Dudhia, J.: A new vertical diffusion package with an explicit treatment of entrainment processes, *Mon. Weather Rev.*, 134, 2318–2341, 2006.
- Im, U., Bianconi, R., Solazzo, E., Kioutsioukis, I., Badia, A., Balzarini, A., Baró, R., Bellasio, R., Brunner, D., Chemel, C., Curci, G., Denier van der Gon, H., Flemming, J., Forkel, R., Giordano, L., Jiménez-Guerrero, P., Hirtl, M., Hodzic, A., Honzak, L., Jorba, O., Knote, C., Makar, P. A., Manders-Groot, A., Neal, L., Pérez, J. L., Pirovano, G., Pouliot, G., San Jose, R., Savage, N., Schroder, W., Sokhi, R. S., Syrakov, D., Torian, A., Tuccella, P., Wang, K., Werhahn, J., Wolke, R., Zabkar, R., Zhang, Y., Zhang, J., Hogrefe, C., and Galmarini, S.: Evaluation of operational online-coupled regional air quality models over Europe and North America in the context of AQMEII phase 2. Part II: Particulate matter, *Atmos. Environ.*, 115, 421–441, doi:10.1016/j.atmosenv.2014.08.072, 2015.
- Jiang, F., Zhou, P., Liu, Q., Wang, T., Zhuang, B., and Wang, X.: Modeling tropospheric ozone formation over East China in springtime, *J. Atmos. Chem.*, 69, 303–319, doi:10.1007/s10874-012-9244-3, 2012.
- Kallos, G., Kassomenos, P., and Pielke, R. A.: Synoptic and mesoscale weather conditions during air pollution episodes in Athens, Greece, *Bound.-Lay. Meteorol.*, 62, 163–184, 1993.
- Kanda, M.: Progress in urban meteorology: A review, *J. Meteorol. Soc. Jpn.*, 85B, 363–383, 2007.
- Kim, H.-J. and Wang, B.: Sensitivity of the WRF model simulation of the East Asian summer monsoon in 1993 to shortwave radi-

- tion schemes and ozone absorption, *Asia-Pac. J. Atmos. Sci.*, 47, 167–180, 2011.
- Kusaka, H. and Kimura, F.: Coupling a single-layer urban canopy model with a simple atmospheric model: Impact on urban heat island simulation for an idealized case, *J. Meteorol. Soc. Jpn.*, 82, 67–80, doi:10.2151/jmsj.82.67, 2004.
- Lei, Y., Zhang, Q., He, K. B., and Streets, D. G.: Primary anthropogenic aerosol emission trends for China, 1990–2005, *Atmos. Chem. Phys.*, 11, 931–954, doi:10.5194/acp-11-931-2011, 2011.
- Li, L., Chen, C. H., Huang, C., Huang, H. Y., Zhang, G. F., Wang, Y. J., Wang, H. L., Lou, S. R., Qiao, L. P., Zhou, M., Chen, M. H., Chen, Y. R., Streets, D. G., Fu, J. S., and Jang, C. J.: Process analysis of regional ozone formation over the Yangtze River Delta, China using the Community Multi-scale Air Quality modeling system, *Atmos. Chem. Phys.*, 12, 10971–10987, doi:10.5194/acp-12-10971-2012, 2012.
- Liao, J., Wang, T., Wang, X., Xie, M., Jiang, Z., Huang, X., and Zhu, J.: Impacts of different urban canopy schemes in WRF/Chem on regional climate and air quality in Yangtze River Delta, China, *Atmos. Res.*, 145, 226–243, 2014.
- Lin, C. Y., Chen, W. C., Chang, P. L., and Sheng, Y. F.: Impact of the Urban Heat Island Effect on Precipitation over a Complex Geographic Environment in Northern Taiwan, *J. Appl. Meteorol. Clim.*, 50, 339–353, doi:10.1175/2010jamc2504.1, 2011.
- Lin, Y.-L., Farley, R. D., and Orville, H. D.: Bulk parameterization of the snow field in a cloud model, *J. Clim. Appl. Meteorol.*, 22, 1065–1092, 1983.
- Liu, Y., Chen, F., Warner, T., and Basara, J.: Verification of a Mesoscale Data-Assimilation and Forecasting System for the Oklahoma City Area during the Joint Urban 2003 Field Project, *J. Appl. Meteorol. Clim.*, 45, 912–929, doi:10.1175/jam2383.1, 2006.
- Liu, Y., Junfeng, L., and Shu, T.: Interannual Variability of Summer-time Aerosol Optical Depth over east asia During 2000–2011: a Potential Influence from el nino Southern Oscillation, *Environ. Res. Lett.*, 8, 044034, doi:10.1088/1748-9326/8/4/044034, 2013.
- Luhar, A. K., Thatcher, M., and Hurley, P. J.: Evaluating a building-averaged urban surface scheme in an operational mesoscale model for flow and dispersion, *Atmos. Environ.*, 88, 47–58, 2014.
- Mage, D., Ozolins, G., Peterson, P., Webster, A., Orthofer, R., Vandeweerd, V., and Gwynne, M.: Urban air pollution in megacities of the world, *Atmos. Environ.*, 30, 681–686, 1996.
- Martilli, A., Clappier, A., and Rotach, M. W.: An urban surface exchange parameterisation for mesoscale models, *Bound.-Lay. Meteorol.*, 104, 261–304, doi:10.1023/a:1016099921195, 2002.
- Miao, S. G., Chen, F., Lemone, M. A., Tewari, M., Li, Q. C., and Wang, Y. C.: An Observational and Modeling Study of Characteristics of Urban Heat Island and Boundary Layer Structures in Beijing, *J. Appl. Meteorol. Clim.*, 48, 484–501, doi:10.1175/2008jamc1909.1, 2009.
- Mlawer, E. J., Taubman, S. J., Brown, P. D., Iacono, M. J., and Clough, S. A.: Radiative transfer for inhomogeneous atmospheres: RRTM, a validated correlated k model for the long-wave, *J. Geophys. Res.-Atmos.*, 102, 16663–16682, 1997.
- Oke, T. R.: *Boundary Layer Climates*, 2nd Edn., Routledge, London, UK, 1987.
- Oke, T. R.: Towards better scientific communication in urban climate, *Theor. Appl. Climatol.*, 84, 179–190, 2006.
- Rosenfeld, D.: Suppression of rain and snow by urban and industrial air pollution, *Science*, 287, 1793–1796, 2000.
- Rotach, M. W., Fisher, B., and Piringier, M.: Cost 715 Workshop on Urban Boundary Layer Parameterizations, *B. Am. Meteorol. Soc.*, 83, 1501–1504, doi:10.1175/bams-83-10-1501, 2002.
- Ryu, Y.-H., Baik, J.-J., Kwak, K.-H., Kim, S., and Moon, N.: Impacts of urban land-surface forcing on ozone air quality in the Seoul metropolitan area, *Atmos. Chem. Phys.*, 13, 2177–2194, doi:10.5194/acp-13-2177-2013, 2013.
- Salamanca, F., Krpo, A., Martilli, A., and Clappier, A.: A new building energy model coupled with an urban canopy parameterization for urban climate simulations-part I. formulation, verification, and sensitivity analysis of the model, *Theor. Appl. Climatol.*, 99, 331–344, doi:10.1007/s00704-009-0142-9, 2010.
- Salamanca, F., Martilli, A., Tewari, M., and Chen, F.: A Study of the Urban Boundary Layer Using Different Urban Parameterizations and High-Resolution Urban Canopy Parameters with WRF, *J. Appl. Meteorol. Clim.*, 50, 1107–1128, doi:10.1175/2010jamc2538.1, 2011.
- Schell, B., Ackermann, I. J., Hass, H., Binkowski, F. S., and Ebel, A.: Modeling the formation of secondary organic aerosol within a comprehensive air quality model system, *J. Geophys. Res.-Atmos.*, 106, 28275–28293, 2001.
- Solazzo, E., Di Sabatino, S., Aquilina, N., Dudek, A., and Britter, R.: Coupling mesoscale modelling with a simple urban model: the Lisbon case study, *Bound.-Lay. Meteorol.*, 137, 441–457, 2010.
- Solazzo, E., Bianconi, R., Pirovano, G., Matthias, V., Vautard, R., Moran, M. D., Wyat Appel, K., Bessagnet, B., Brandt, J., Christensen, J. H., Chemel, C., Coll, I., Ferreira, J., Forkel, R., Francis, X. V., Grell, G., Grossi, P., Hansen, A. B., Miranda, A. I., Nopmongkol, U., Prank, M., Sartelet, K. N., Schaap, M., Silver, J. D., Sokhi, R. S., Vira, J., Werhahn, J., Wolke, R., Yarwood, G., Zhang, J., Rao, S. T., and Galmarini, S.: Operational model evaluation for particulate matter in Europe and North America in the context of AQMEII, *Atmos. Environ.*, 53, 75–92, doi:10.1016/j.atmosenv.2012.02.045, 2012.
- Souch, C. and Grimmond, S.: Applied climatology: urban climate, *Prog. Phys. Geogr.*, 30, 270–279, 2006.
- Tie, X., Madronich, S., Li, G., Ying, Z., Zhang, R., Garcia, A. R., Lee-Taylor, J., and Liu, Y.: Characterizations of chemical oxidants in Mexico City: A regional chemical dynamical model (WRF-Chem) study, *Atmos. Environ.*, 41, 1989–2008, 2007.
- Tie, X., Geng, F., Guenther, A., Cao, J., Greenberg, J., Zhang, R., Apel, E., Li, G., Weinheimer, A., Chen, J., and Cai, C.: Megacity impacts on regional ozone formation: observations and WRF-Chem modeling for the MIRAGE-Shanghai field campaign, *Atmospheric Chemistry and Physics*, 13, 5655–5669, doi:10.5194/acp-13-5655-2013, 2013.
- Trusilova, K., Früh, B., Brienen, S., Walter, A., Masson, V., Pigeon, G., and Becker, P.: Implementation of an Urban Parameterization Scheme into the Regional Climate Model COSMO-CLM, *J. Appl. Meteorol. Clim.*, 52, 2296–2311, doi:10.1175/JAMC-D-12-0209.1, 2013.
- Wang, J., Feng, J., Yan, Z., Hu, Y., and Jia, G.: Nested high-resolution modeling of the impact of urbanization on regional climate in three vast urban agglomerations in China, *J. Geophys. Res.-Atmos.*, 117, D21103, doi:10.1029/2012JD018226, 2012.

- Wang, M. N., Zhang, X. Z., and Yan, X. D.: Modeling the climatic effects of urbanization in the Beijing-Tianjin-Hebei metropolitan area, *Theor. Appl. Climatol.*, 113, 377–385, doi:10.1007/s00704-012-0790-z, 2013.
- Wang, X., Wu, Z., and Liang, G.: WRF/CHEM modeling of impacts of weather conditions modified by urban expansion on secondary organic aerosol formation over Pearl River Delta, *Particuology*, 7, 384–391, doi:10.1016/j.partic.2009.04.007, 2009.
- Wang, X., Zhang, Y., Hu, Y., Zhou, W., Lu, K., Zhong, L., Zeng, L., Shao, M., Hu, M., and Russell, A. G.: Process analysis and sensitivity study of regional ozone formation over the Pearl River Delta, China, during the PRIDE-PRD2004 campaign using the Community Multiscale Air Quality modeling system, *Atmos. Chem. Phys.*, 10, 4423–4437, doi:10.5194/acp-10-4423-2010, 2010.
- Wang, Z.-H., Bou-Zeid, E., and Smith, J. A.: A spatially-analytical scheme for surface temperatures and conductive heat fluxes in urban canopy models, *Bound.-Lay. Meteorol.*, 138, 171–193, 2011.
- Wesely, M.: Parameterization of surface resistances to gaseous dry deposition in regional-scale numerical models, *Atmos. Environ.*, 23, 1293–1304, 1989.
- Yang, B., Zhang, Y. C., and Qian, Y.: Simulation of urban climate with high-resolution WRF model: A case study in Nanjing, China, *Asia-Pac. J. Atmos. Sci.*, 48, 227–241, doi:10.1007/s13143-012-0023-5, 2012.
- Yang, Z. and Shiang-Yuh, W.: Understanding of the Fate of Atmospheric Pollutants Using a Process Analysis Tool in a 3-D Regional Air Quality Model at a Fine Grid Scale, *Atmos. Clim. Sci.*, 3, 18–30, doi:10.4236/acs.2013.31004, 2013.
- Yoshikado, H. and Tsuchida, M.: High levels of winter air pollution under the influence of the urban heat island along the shore of Tokyo Bay, *J. Appl. Meteorol.*, 35, 1804–1813, doi:10.1175/1520-0450(1996)035<1804:hlowap>2.0.co;2, 1996.
- Yu, M., Carmichael, G. R., Zhu, T., and Cheng, Y. F.: Sensitivity of predicted pollutant levels to urbanization in China, *Atmos. Environ.*, 60, 544–554, doi:10.1016/j.atmosenv.2012.06.075, 2012.
- Zhang, L. and He, Z.: Technical Note: An empirical algorithm estimating dry deposition velocity of fine, coarse and giant particles, *Atmos. Chem. Phys.*, 14, 3729–3737, doi:10.5194/acp-14-3729-2014, 2014.
- Zhang, N., Gao, Z. Q., Wang, X. M., and Chen, Y.: Modeling the impact of urbanization on the local and regional climate in Yangtze River Delta, China, *Theor. Appl. Climatol.*, 102, 331–342, doi:10.1007/s00704-010-0263-1, 2010.
- Zhang, Q., Streets, D. G., Carmichael, G. R., He, K. B., Huo, H., Kannari, A., Klimont, Z., Park, I. S., Reddy, S., Fu, J. S., Chen, D., Duan, L., Lei, Y., Wang, L. T., and Yao, Z. L.: Asian emissions in 2006 for the NASA INTEX-B mission, *Atmos. Chem. Phys.*, 9, 5131–5153, doi:10.5194/acp-9-5131-2009, 2009.